Proceedings of the ASME 2013 International Design Engineering Technical Conferences & Conference on Mechanical Vibration and Noise
IDETC/VIB 2013
August 04-07, 2013, Portland, OR, USA

DETC2013-13198

GLOBAL "ECLIPSE" BIFURCATION IN A TWINKLING OSCILLATOR

Smruti R. Panigrahi*
Dynamics and Vibrations
Research Laboratory
Dept. of Mechanical Engineering
Michigan State University
E. Lansing, Michigan, 48824
Email: smruti@msu.edu
Phone: 517-515-1620

Brian F. Feeny
Dept. of Mechanical Engineering
Michigan State University
E. Lansing, Michigan, 48824
Email: feeny@egr.msu.edu
Phone: 517-353-9451
Fax: 517-353-1750

Alejandro R. Diaz
Dept. of Mechanical Engineering
Michigan State University
E. Lansing, Michigan, 48824
Email: diaz@egr.msu.edu
Phone: 517-353-9861
Fax: 517-353-1750

ABSTRACT

This work regards the use of cubic springs with intervals of negative stiffness, in other words "snap-through" elements, in order to convert low-frequency ambient vibrations into high-frequency oscillations, referred to as "twinkling". The focus of this paper is on a global bifurcation of a two-mass chain which, in the symmetric system, involves infinitely many equilibria at the bifurcation point. The structure of this "eclipse" bifurcation is uncovered, and perturbations of the bifurcation are studied. The energies associated with the equilibria are examined.

Keywords: *negative stiffness, twinkling oscillators, snap-through structures, star bifurcation, codimension, eclipse bifurcation*

1 Introduction

Nonlinearity has been studied by several authors for energy management. For example, essential nonlinearity has been used for nonlinear energy pumping [1–3], nonlinear targeted energy transfer (TET) [4–8], and as a nonlinear energy sink (NES) for energy harvesting [9–11]. Indeed, vibration based energy harvesting has been studied for linear and nonlinear systems [12–22]. Novel ways of experimental energy harvesting have been achieved from low frequency ambient excitations [18, 19, 23, 24].

This work is motivated by the idea of using snap-through structures to induce high frequency oscillations from low frequency ambient vibrations such as low-frequency seismic phenomena, tsunamis and low-frequency ocean waves, to harvest energy. Several authors have studied the dynamics of various snap-through negative stiffness and bistable systems [25–29]. Nonlinear massless static electric-springs [30], and magneto static-springs [31] have been studied numerically.

We explore the dynamics of a nonlinear mass chain with cubic springs that have three distinct roots in the characteristic. The chain is connected to a fixed base at one end and to a pulled point at the other end, as shown in Figure 1. The end spring is then pulled quasistatically to a certain distance to observe the "twinkling phenomenon" in the chain. As this pull parameter is changed we see high frequency oscillations about different equilibrium states. As the system exhibits twinkling phenomenon and comes to an equilibrium state due to small applied damping, it contains a total energy that was not present in the system before the applied quasistatic pull. This residual energy will be of importance to energy harvesting.

The two degree of freedom (DOF) twinkling oscillator exhibits complicated bifurcation behaviors as seen in [32, 33] where we have discussed the observed, *star bifurcation*, in detail. The undamped star bifurcation is observed to be a codimension-four bifurcation where four zero eigenvalues were found in the symmetric case. Various types of perturbations revealed the symmetry breaking bifurcation behavior of the star bifurcation.

*Address all correspondence to this author.

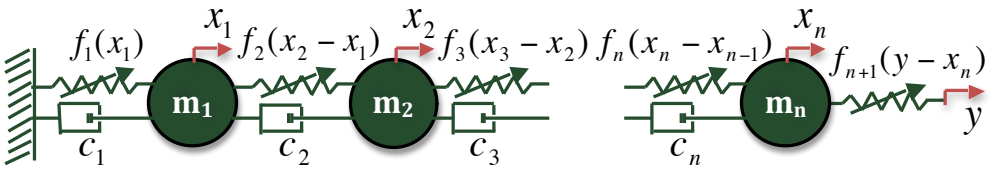

FIGURE 1: n-degree-of-freedom spring-mass chain connected by n masses, $(n+1)$ nonlinear springs, and n dash-pots. As shown in this figure the left spring is fixed to a base and the right most spring is pulled quasistatically to a distance y_0.

The star bifurcation occurs when the twinkler enters a negative stiffness region with respect to the quasistatic pull parameter y_0. We have also identified another new type of bifurcation as the twinkler passes through the negative stiffness regime. We call this bifurcation as "*eclipse bifurcation*".

Many different equilibrium configurations can coexist for a simple two-DOF model. Final equilibria of this type of twinkler have differing energy states. Predicting the final energy of the system requires analysis of transients, which are influenced by the structure of both stable and unstable equilibria. In this work we first formulate a non-dimensionalized *normal form* in order to study the eclipse bifurcation behavior of 2-DOF system in detail. While the system goes through the eclipse bifurcation, it exhibits infinitely many equilibria whose stability will be determined. The behavior of these equilibria will be discussed in this article. The stability analysis and the related degree of degeneracy are studied using the concept of codimension [34, 35], and show how the codimension of the system changes with damping.

In section 2, we review the nonlinear equation of motion, and conditions for the stability as discussed in [32, 33]. In section 3 and 4, we will perform a coordinate transformation and obtain a normal form for the global bifurcation and eclipse bifurcation respectively in a 2-DOF system.

2 Snap-Through Structures: Twinkler

The equations of motion of an n-degree-of-freedom snap-through system as shown in the Figure 1, written using the Newton's second law of motion have the form

$$\ddot{\mathbf{x}} + \mathbf{C}\dot{\mathbf{x}} = \mathbf{F}(\mathbf{x}) \tag{1}$$

where $\mathbf{x}$ and $\mathbf{F}(\mathbf{x})$ are $n \times 1$ array of mass displacements and $n \times 1$ array of spring force respectively. For example $F^j(x_{j-1}, x_j, x_{j+1}) = f_{j+1}(x_{j+1} - x_j) - f_j(x_j - x_{j-1})$, where $j = 2, 3, \ldots n-1$ and F^j is the j^{th} element of spring force vector $\mathbf{F}$. Also we can split the total spring force into two parts as $\mathbf{F}(\mathbf{x}) = -\mathbf{K}\mathbf{x} + \mathbf{f}_{nl}$ with $(-\mathbf{K}\mathbf{x})$ as the linear and $\mathbf{f}_{nl}$ as the nonlinear part of the spring force. In this case $\mathbf{K}$ is a linear stiffness coefficient matrix. We consider a cubic spring with the spring force $f_i(s_i)$ to be of the form

$$f_i(s_i) = \gamma_i s_i (s_i - a_i)(s_i - b_i); \quad \forall\, i = 1, 2, \ldots, n+1 \tag{2}$$

where, $s_i = x_i - x_{i-1}$ is the spring deformation. Referring to Figure 3, for the end spring held at $y = y_0$, we examine the equilibria. At equilibrium, the accelerations and the velocities of all the masses are zero. Hence we get the following array of equilibrium equations for the n-DOF structure:

$$\begin{aligned} f_2(x_2 - x_1) &= f_1(x_1) \\ f_{i+1}(x_{i+1} - x_i) &= f_i(x_i - x_{i-1}); \quad \forall\, i = 2, 3, \ldots, n-1 \\ f_{n+1}(y_0 - x_n) &= f_n(x_n - x_{n-1}) \end{aligned} \tag{3}$$

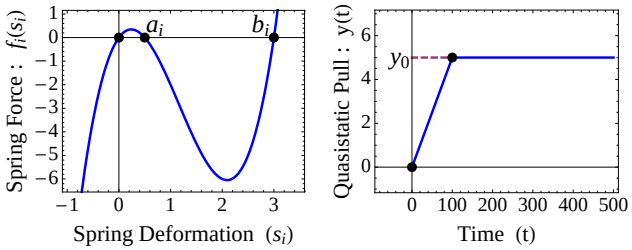

FIGURE 2: The characteristic spring force $f_i(s_i)$ of the nonlinear spring as a function of the spring deformation s_i, and the quasistatic pull as a function of time.

As we solve equation (3) we find the bifurcation behavior with respect to y_0. The stabilities of the equilibria of the set of second-order ordinary differential equations (1) can be found by computing the eigenvalues of the Jacobian of $\mathbf{F}$. We first let $\hat{\mathbf{x}} = \mathbf{x} - \bar{\mathbf{x}}$, where $\bar{\mathbf{x}}$ is the equilibrium point. Then we write the linearized system in second-order form as

$$\ddot{\hat{\mathbf{x}}} = [\mathbf{DF}]\hat{\mathbf{x}} = -\tilde{\mathbf{K}}\hat{\mathbf{x}} \;\Rightarrow \ddot{\hat{\mathbf{x}}} + \tilde{\mathbf{K}}\hat{\mathbf{x}} = \mathbf{0} \tag{4}$$

Assuming a response of the form $\hat{\mathbf{x}} = e^{\pm i\omega t}\underline{\phi}$, the eigenvalue problem becomes

$$\left[\tilde{\mathbf{K}} - \lambda I\right] \underline{\phi} = 0 \Rightarrow \lambda = \omega^2 \tag{5}$$

where ω are the eigenfrequencies, λ are the eigenvalues and $\underline{\phi}$ are the eigenvectors. If $\lambda < 0$ there is an exponential solution that blows up as time t increases. A stable oscillatory solution exists for $\lambda > 0$, and neutrally stable solutions for $\lambda = 0$.

Thus, in the second-order undamped form, a bifurcation is indicated as a single eigenvalue passes through zero, corresponding to a transition of a second-order oscillation to a second-order saddle (in a two-dimensional phase space). Equivalently, it corresponds to an effective stiffness going from positive to negative.

For analysis of the codimension as discussed in [32, 33], the second-order ordinary differential equations for the n-DOF system are converted into first-order differential equations by defining a $2n \times 1$ state vector $\mathbf{z} = \begin{pmatrix} \dot{\mathbf{x}} \\ \mathbf{x} \end{pmatrix}$ yielding unforced EOM of the form

$$\mathbf{A}\dot{\mathbf{z}} = \mathbf{L}\mathbf{z} + \tilde{\mathbf{f}} \tag{6}$$

$$\text{where} \quad \mathbf{A} = \begin{bmatrix} \mathbf{M} & \mathbf{0} \\ \mathbf{0} & \mathbf{I} \end{bmatrix}, \quad \mathbf{L} = \begin{bmatrix} -\mathbf{C} & -\mathbf{K} \\ \mathbf{I} & \mathbf{0} \end{bmatrix}, \quad \tilde{\mathbf{f}} = \begin{pmatrix} \mathbf{f}_{nl} \\ \mathbf{0} \end{pmatrix} \tag{7}$$

$\mathbf{A}$ and $\mathbf{L}$ are $2n \times 2n$ matrices and $\tilde{\mathbf{f}}$ is $2n \times 1$ vector. The state-variable system can be linearized about an equilibrium and put in the form $\dot{\mathbf{z}} = \mathbf{T}\mathbf{z}$. For $i = 1, 2, \ldots, 2n$, the signs of the real parts of the eigenvalues, α_i, from the eigenvalue problem $\mathbf{T}\mathbf{u} = \alpha\mathbf{u}$ indicate stability.

In the following analyses, we use λ to indicate eigenvalues from the undamped second-order-set formulation (equation (4)), and α to represent the eigenvalues from the linearization of the general state-variable description (equation (6)).

3 Bifurcations in 2-DOF Twinkler

The cubic nonlinearity in the twinkler gives rise to multiple equilibria for the parameter region where the twinkler passes through the negative stiffness region. We used a coordinate transformation to simplify and nondimensionalize the EOMs for the analysis of the bifurcation events. For 2-DOF twinkler (Figure 3) we obtain the equilibria from equation (3) with $n = 2$. For the symmetric case, all the springs are identical. Hence $\gamma_i = \gamma$, $a_i = a$ and $b_i = b$. For computations, we have used $\gamma = 2$, $a = 0.5$, and $b = 3.0$. The values of a and b are chosen to represent a stiffness function of a spring that is preloaded to be somewhat near snap through.

The steady-state dynamics of the 2-DOF system is considered in order to understand the various possible equilibria that exist due to the coupling of the snap-through elements with the equilibrium conditions $f_1(x_1) = f_2(x_2 - x_1)$ and $f_2(x_2 - x_1) = f_3(y_0 - x_2)$. We transform the coordinates to simplify the EOM, using $y_0 = \tilde{p} + y_b$, $x_1 = \tilde{u}_1 + \frac{\tilde{p}+y_b}{3}$, and $x_2 = \tilde{u}_2 + \frac{2(\tilde{p}+y_b)}{3}$, where $y_b = a + b - \sqrt{a^2 - ab + b^2}$ as discussed in [32, 33]. We obtain

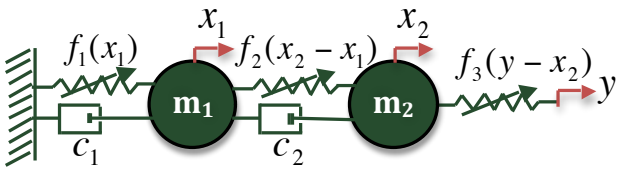

FIGURE 3: 2-degree-of-freedom spring-mass chain connected by 2 masses, 3 nonlinear springs, and 2 dash-pots. The left spring is fixed to a base and the right most spring is pulled quasistatically to a distance y_0.

$$\begin{aligned} \ddot{\tilde{u}}_1 + 2\tilde{c}\dot{\tilde{u}}_1 - \tilde{c}\dot{\tilde{u}}_2 &= 2\left(\tilde{u}_2 - 2\tilde{u}_1\right)\left(\tilde{A}(\tilde{u}_1, \tilde{u}_2) - \tilde{u}_2 y_1 + \tilde{p}\tilde{u}_2\right) \\ \ddot{\tilde{u}}_2 - \tilde{c}\dot{\tilde{u}}_1 + \tilde{c}\dot{\tilde{u}}_2 &= 2\left(\tilde{u}_1 - 2\tilde{u}_2\right)\left(\tilde{A}(\tilde{u}_1, \tilde{u}_2) + \tilde{u}_1 y_1 - \tilde{p}\tilde{u}_1\right) \end{aligned} \tag{8}$$

where $\tilde{A}(\tilde{u}_1, \tilde{u}_2) = \left(\tilde{u}_1^2 - \tilde{u}_1\tilde{u}_2 + \tilde{u}_2^2 - \frac{2\tilde{p}y_1}{3} + \frac{\tilde{p}^2}{3}\right)$, and $y_1 = (a + b - y_b)$. Introducing non-dimensional variables (p, u_1, u_2, τ, c), such that $t = \tau \frac{3}{y_1\sqrt{2}}$, $\tilde{p} = p\frac{y_1}{3}$, $\tilde{u}_1 = u_1\frac{y_1}{3}$, $\tilde{u}_2 = u_2\frac{y_1}{3}$, and $\tilde{c} = c\, y_1 \frac{\sqrt{2}}{3}$, the above equation is simplified to obtain nondimensionalized global equilibrium equations for the 2-DOF twinkler as

$$\begin{aligned} \ddot{u}_1 + 2c\dot{u}_1 - c\dot{u}_2 &= (u_2 - 2u_1)\left(A(u_1, u_2) - 3u_2 + pu_2\right) \\ \ddot{u}_2 - c\dot{u}_1 + c\dot{u}_2 &= (u_1 - 2u_2)\left(A(u_1, u_2) + 3u_1 - pu_1\right) \end{aligned} \tag{9}$$

where $A(u_1, u_2) = \left(u_1^2 - u_1u_2 + u_2^2 - 2p + \frac{p^2}{3}\right)$, $\dot{u}_i = \frac{du_i}{d\tau}$, and $\ddot{u}_i = \frac{d^2u_i}{d\tau^2}$. At equilibrium $\ddot{u}_1 = \ddot{u}_2 = 0$, $\dot{u}_1 = \dot{u}_2 = 0$. Therefore the equilibrium condition for the 2-DOF twinkler is

$$\begin{aligned} g_1(u_1, u_2, p) &= (u_2 - 2u_1)\left(A(u_1, u_2) - 3u_2 + pu_2\right) = 0 \\ g_2(u_1, u_2, p) &= (u_1 - 2u_2)\left(A(u_1, u_2) + 3u_1 - pu_1\right) = 0 \end{aligned} \tag{10}$$

The solutions to the above equilibrium equations are

$$\begin{aligned} (u_1, u_2) = \{&(0,0),\ (-2p_1, -p_1),\ (-2p_2, -p_2), \\ &(p_1, -p_1),\ (p_2, -p_2),\ (p_2, 2p_2),\ (p_1, 2p_1)\} \end{aligned} \tag{11}$$

where $p_1 = \frac{1}{6}\left(p - 3 + \sqrt{9 + 18p - 3p^2}\right)$ and $p_2 = \frac{1}{6}\left(p - 3 - \sqrt{9 + 18p - 3p^2}\right)$, which have elliptical solution curves as shown in Figure 4. These expressions were

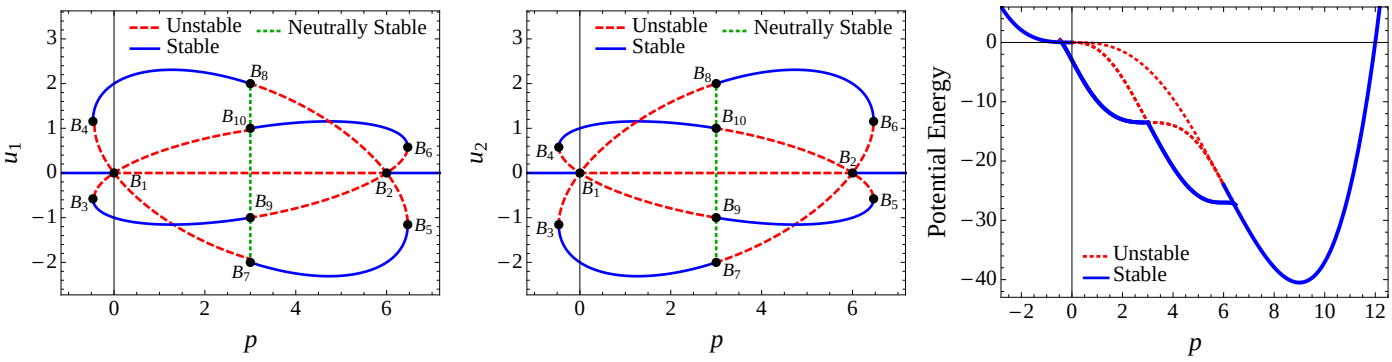

(a) projection on $p-u_1$ plane (b) projection on $p-u_2$ plane (c) spring potential

FIGURE 4: The bifurcation diagram for the equilibrium solutions of the lightly damped symmetric 2-DOF system with respect to the pull parameter y_0, where $B_1, B_2, \ldots, B_{10}$ are the bifurcation points. The dashed lines represent unstable solutions, and the solid lines represent the stable equilibrium solutions (neutrally stable for the undamped system). The vertical dotted lines show infinitely many solutions at $p = 3$ (or $y_0 = a + b$), where at the bifurcation points $B_7 - B_{10}$, two of the four eigenvalues, α, are complex conjugates with zero real parts and the other two are zero for the undamped system, whereas with light damping there is one zero, one purely real negative, and the other two are complex conjugate eigenvalues with negative real parts. The bifurcation points $B_3 - B_6$, are saddle-nodes. With no damping two zero and two complex conjugate eigenvalues with zero real parts for the undamped system, and with light damping there are two complex conjugate eigenvalues with negative real parts, one zero, and one purely real negative eigenvalues. Figure (c) represents the total final potential energy of the 2-DOF symmetric system as a function of p. For a given value of p, all stable solutions have the same potential energy in the symmetric system.

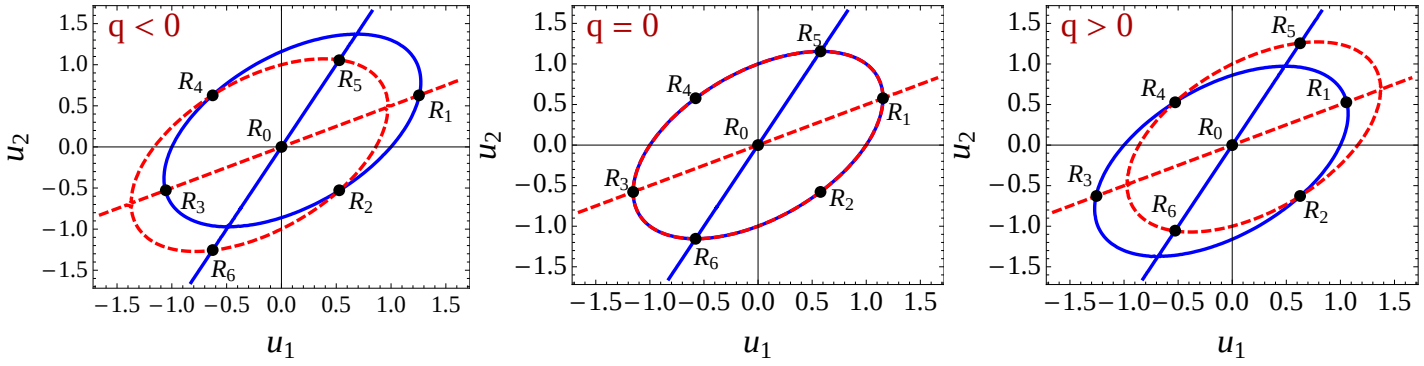

FIGURE 5: The equilibrium solutions projected onto the (u_1, u_2) plane and noted as $R_j = (u_1, u_2)_j$, for $j = 0, 1, 2, \cdots, 6$. The solid and dashed ellipses and straight lines satisfy $h_1(u_1, u_2, q) = 0$ and $h_2(u_1, u_2, q) = 0$ respectively. As q approaches zero from both directions, the two ellipses coincide, resulting in an infinite number of solutions on the ellipse. All the solutions on the ellipse are marginally stable.

obtained using the "Solve" command in MATHEMATICA. The stabilities of the equilibria curves are determined from the eigenvalues, λ, as discussed in equations (4) and (5). The "base line" solution $(0,0)$ in the u variables (the horizontal lines in Figure 4 (a), (b)) corresponds to the diagonal lines in the original coordinates given by $x_1 = \frac{py_1+3y_b}{9}$ and $x_2 = \frac{2(py_1+3y_b)}{9}$.

As p increases, the baseline solution destabilizes in a bifurcation that features a collision of four branches of equilibria on either side of the bifurcation point B_1. Three branches are visible on either side of the bifurcation point in each figure because vertical axis of these figures is a projection of a higher dimensional phase space, and some curves overlap in each projection. In each plot in Figure 4, the narrow elliptical curve of equilibria is actually two overlapping elliptical curves. For convenience, we referred to this bifurcation as a "*star bifurcation*", as eight branches (two overlap in the Figure) emanate from the bifurcation point, in which a neutrally stable (asymptotically stable when light damping is applied) curve collides simultaneously with three unstable curves to produce four unstable curves. (See [32, 33] for more

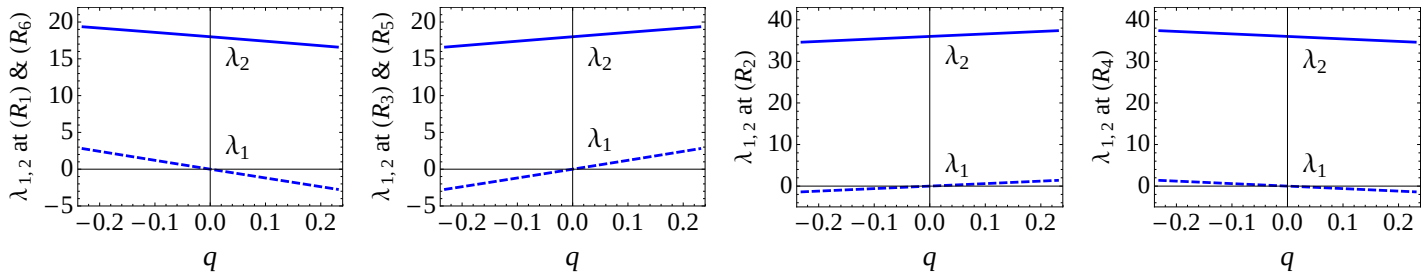

FIGURE 6: The vertical axis represents the eigenvalues at the equilibria in the normal form at the eclipse bifurcation local to $q = 0$. For $q < 0$ the points R_1, R_4 and R_6 are stable and become unstable when $q > 0$ where as R_2, R_3 and R_5 changes from unstable to unstable as q goes from negative to positive and R_0 remain unstable on both sides local to $q = 0$.

details.)

At $p = 3$ (or $\tilde{p} = y_1$), the equilibria on the elliptical curves undergo an exchange of stability without intersection as seen in Figure 4. There exists an infinite number of equilibria at this particular value of p. We will look at the structure of this bifurcation next.

4 Eclipse Bifurcation

Now we look closely at the degenerate exchange of stability bifurcation at $p = 3$ or $\tilde{p} = y_1 = 2.7838$. We consider the EOM local to $\tilde{p} = y_1$. Letting $\tilde{p} = y_1 + \tilde{q}$ in equation (8) we get

$$\begin{aligned}
&\ddot{\tilde{u}}_1 + 2\tilde{c}\dot{\tilde{u}}_1 - \tilde{c}\dot{\tilde{u}}_2 \\
&\quad = 2(\tilde{u}_2 - 2\tilde{u}_1)\left(\tilde{u}_1^2 - \tilde{u}_1\tilde{u}_2 + \tilde{u}_2^2 + \tilde{q}\tilde{u}_2 - \frac{y_1^2}{3} + \frac{\tilde{q}^2}{3}\right) \\
&\ddot{\tilde{u}}_2 - \tilde{c}\dot{\tilde{u}}_1 + \tilde{c}\dot{\tilde{u}}_2 \\
&\quad = 2(\tilde{u}_1 - 2\tilde{u}_2)\left(\tilde{u}_1^2 - \tilde{u}_1\tilde{u}_2 + \tilde{u}_2^2 - \tilde{q}\tilde{u}_1 - \frac{y_1^2}{3} + \frac{\tilde{q}^2}{3}\right)
\end{aligned} \tag{12}$$

For the eclipse bifurcation we consider solutions very close to the bifurcation points. I.e. $\tilde{q}$ is of order ε. So $\tilde{q}^2$ is on the order of ε^2. Hence neglecting $\tilde{q}^2$ terms, and letting $t = \tau\,\frac{\sqrt{3}}{y_1\sqrt{2}}$, $\tilde{q} = q\frac{y_1}{\sqrt{3}}$, $\tilde{u}_1 = u_1\frac{y_1}{\sqrt{3}}$, $\tilde{u}_2 = u_2\frac{y_1}{\sqrt{3}}$, and $\tilde{c} = c\,y_1\frac{\sqrt{2}}{\sqrt{3}}$, the above equations are simplified to obtain a non-dimensionalized normal form of the equations for the eclipse bifurcation:

$$\begin{aligned}
&\ddot{u}_1 + 2c\dot{u}_1 - c\dot{u}_2 = h_1(u_1,u_2,q) \\
&\quad = (u_2 - 2u_1)\left(u_1^2 - u_1u_2 + u_2^2 + qu_2 - 1\right) \\
&\ddot{u}_2 - c\dot{u}_1 + c\dot{u}_2 = h_2(u_1,u_2,q) \\
&\quad = (u_1 - 2u_2)\left(u_1^2 - u_1u_2 + u_2^2 - qu_1 - 1\right)
\end{aligned} \tag{13}$$

At equilibrium both of these equations represent a straight curve and an ellipse in u_1, u_2 space. The dashed and solid ellipses and straight lines in Figure 5 satisfy $h_1(u_1,u_2,q) = 0$ and $h_2(u_1,u_2,q) = 0$ of equation (13) respectively. The intersections between a solid curve and a dashed curve satisfy both of equations (13), and are therefore the equilibria (u_1,u_2), denoted by R_0, R_1,..., R_6. At $q = 0$, both ellipses overlap perfectly in the symmetric system, producing an elliptic locus of infinitely many equilibria. We refer to this as an "*eclipse bifurcation*".

Now we examine the stability of equilibria. The equilibrium solution to equations (13) are

$$\begin{aligned}
(u_1,u_2) = \Big\{&R_0 : (0,0);\ R_1 : (-2r_2,-r_2);\ R_2 : (r_1,-r_1); \\
&R_3 : (-2r_1,-r_1);\ R_4 : (r_2,-r_2); \\
&R_5 : (r_1,2r_1);\ R_6 : (r_2,2r_2)\Big\}
\end{aligned} \tag{14}$$

where $r_1 = \frac{1}{6}\left(q + 2\sqrt{3}\right)$ and $r_2 = \frac{1}{6}\left(q - 2\sqrt{3}\right)$.

The Jacobian of the second-order undamped ($c_1 = c_2 = 0$) form of equations (13) is computed from $\mathbf{J} = -\mathbf{Dh}$, where $\mathbf{h} = [h_1(u_1,u_2), h_2(u_1,u_2)]^T$, as in

$$\mathbf{J} = \begin{bmatrix} 2(u_2 - 2u_1)^2 & 2(u_1 - 2u_2)(u_2 - 2u_1) \\ 2(u_1 - 2u_2)(u_2 - 2u_1) & 2(u_1 - 2u_2)^2 \end{bmatrix} \tag{15}$$

The eigenvalues of the above Jacobian, at the equilibria obtained in the equation (14), are illustrated in Figure 6. The Jacobian has the following characteristic equation:

$$\lambda^2 - 2\lambda\left(5u_1^2 - 8u_1u_2 + 5u_2^2\right) = 0 \tag{16}$$

The eigenvalues at the equilibria from equation (14) are $\lambda_1 = 0$, and $\lambda_2 = 0,\ 18r_2^2,\ 36r_1^2,\ 18r_1^2,\ 36r_2^2,\ 18r_1^2,\ 18r_2^2$ for R_0 to R_6 respectively. With $\lambda_1 = 0$ and $\lambda_2 \geq 0$ at all of these equilibria we conclude the solutions to be marginally stable. The bifurcations of the equilibria in the unperturbed system are shown in Figure 7(a).

To examine the stabilities of the equilibrium solutions lying on the overlapping ellipses $\left(u_1^2 - u_1u_2 + u_2^2 - 1\right) = 0$, from equation (13) at $q = 0$, we replace $u_1u_2 = \left(u_1^2 + u_2^2 - 1\right)$ in

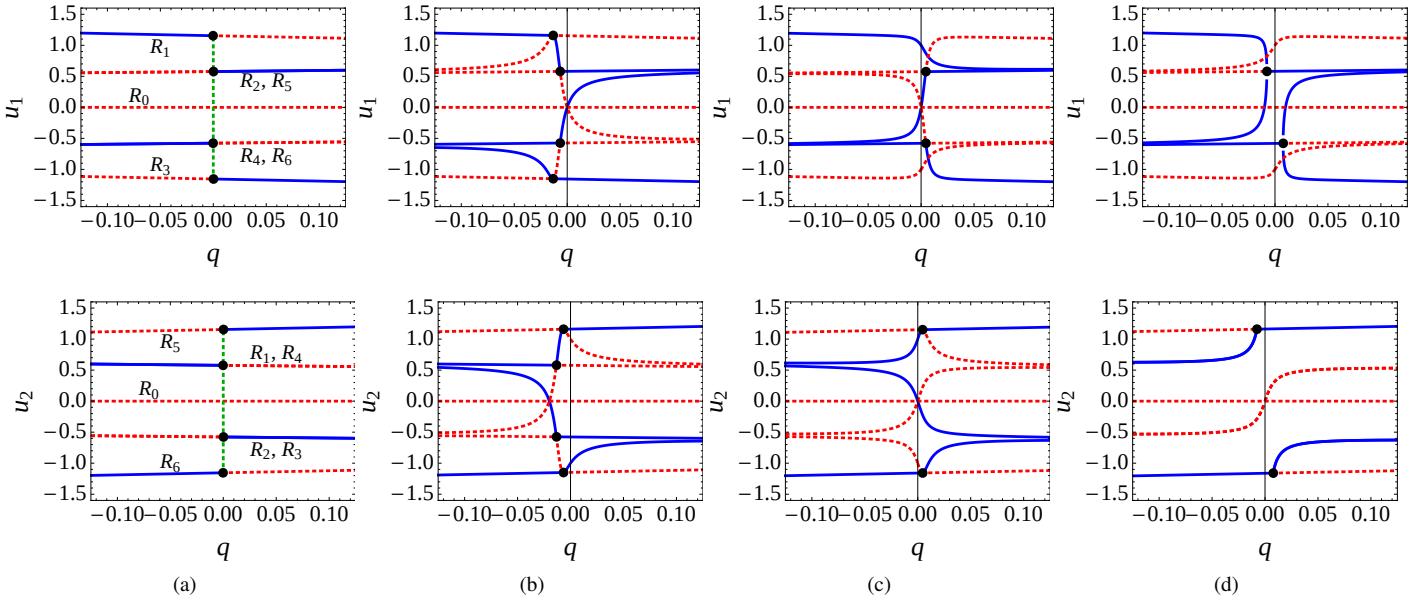

FIGURE 7: Symmetric case and three different symmetry-breaking bifurcations are presented. The solid and dashed curves represent the stable and unstable branches respectively and the dots represent the bifurcation points. Top and bottom rows show the projections on $\hat{u}_1 - \hat{q}$, and $\hat{u}_2 - \hat{q}$ planes respectively. The first two symmetry-breaking cases unfold the eclipse bifurcation into transcritical bifurcations and the last figure shows the breaking of the eclipse into stiff pitchfork bifurcations. (a) is the symmetric case. The broken symmetry in (b) results in four transcritical bifurcations, while that in (c) results in two transcritical bifurcations, and that of (d) results in stiff pitchforks.

equation (16), to obtain the new characteristic equation

$$\lambda^2 + 6\lambda\left(u_1^2 + u_2^2 - \frac{8}{3}\right) = 0 \tag{17}$$

Hence $\lambda_1 = 0$, and $\lambda_2 = -6(u_1^2 + u_2^2 - \frac{8}{3})$. Therefore $\lambda_2 > 0$ if the equilibrium solutions (u_1, u_2) on the overlapping ellipses lie inside the circle of radius $\frac{2\sqrt{2}}{\sqrt{3}}$. Since the major and minor radius of the ellipses are $\sqrt{2}$ and $\frac{\sqrt{2}}{\sqrt{3}}$ respectively and both are less than the radius of the circle, all of the solutions on the ellipses are contained inside the circle of radius $\frac{2\sqrt{2}}{\sqrt{3}}$ (Figure 8). Hence we have $\lambda_1 = 0$ and $\lambda_2 > 0$ at $q = 0$, i.e. all of these infinitely many solutions are marginally stable. At $q = 0$, the the symmetric system therefore exhibits a codimension-two eclipse bifurcation.

A global bifurcation behavior is presented in Figure 9, for a particular symmetry-breaking example, revealing the overlapped branches on the (p, u_1) and (p, u_2) planes. Now to reveal the degeneracy at the eclipse bifurcation point, we apply a small perturbation to the normal form, which results in the breaking and unfolding of the eclipse bifurcation. The local normal form is studied for various types of perturbations on both (q, u_1) and (q, u_2) planes as shown in Figures 7(b)-(d). We observed from the various perturbations that the eclipse bifurcation changes

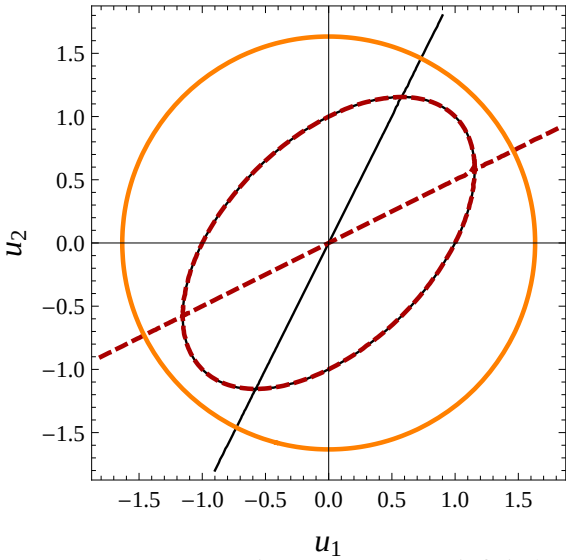

FIGURE 8: For symmetric system at $q = 0$, infinitely many equilibria exist on the overlapping ellipses that are contained within the circle of radius $\frac{2\sqrt{2}}{\sqrt{3}}$. This circle is used as a criterion to determine that these equilibria are marginally stable.

to saddle-node, stiff pitchfork and transcritical bifurcations depending on the perturbation type, the later two of which can

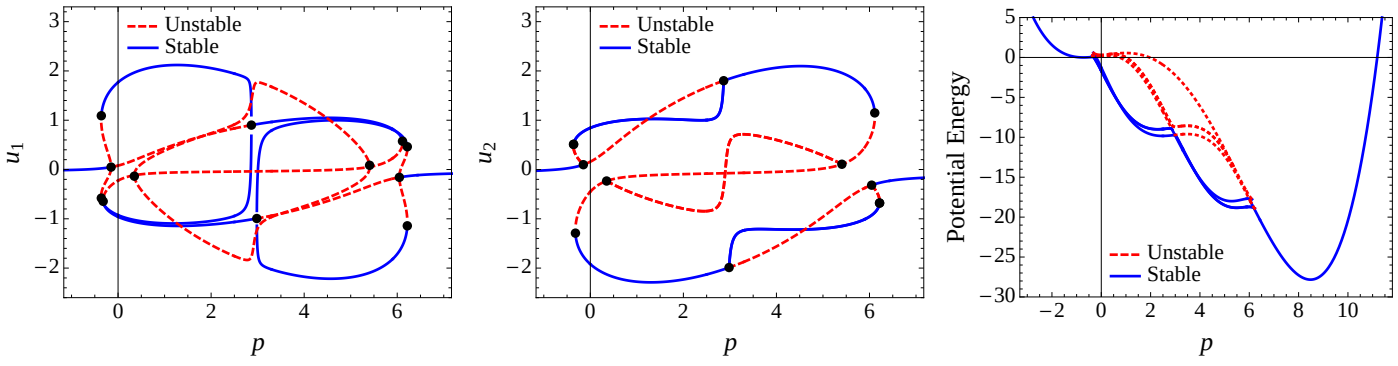

(a) projection on $p-u_1$ plane (b) projection on $p-u_2$ plane (c) spring potential

FIGURE 9: (a)-(b) The global bifurcation diagram for the equilibrium solutions on $p-\mathrm{u}_1$ and $p-u_2$ plane, in one of the symmetry breaking configurations. The perturbation is applied such that the spring force of the end spring is perturbed by making $a_3 = a+\varepsilon$ and $b_3 = b+\varepsilon$, for small epsilon. We have taken $\varepsilon = 0.1$, to show the symmetry breaking more clearly. The star bifurcation at $\tilde{p} = 0$ and the eclipse bifurcation at $\tilde{p} = y_1$, are unfolded revealing one of the configurations of the global perturbations. Figure (c) shows the corresponding global energy levels in the perturbed system.

be further reduced to saddle-nodes with additional perturbations. Also the overlapping branches at u_1 and u_2 equal to ± 0.5, are revealed with the perturbations. We observe that with the symmetry breaking, some parts of the locus of neutrally stable equilibria at $q = 0$ in the symmetric case are changed to stable and some to unstable.

The global bifurcation diagram for the energy provides insight into the optimum harvestable energy in the pull parameter region. Multiple energy levels exist in the negative stiffness region for the symmetry breaking case as seen in Figure 9(c). At a particular value of the pull parameter p in the negative stiffness region, depending on different initial conditions or different parameter values such as the mass and damping coefficients, the final energy lands on one of those levels. Therefore predicting the highest levels of harvestable energies in this region is difficult. However this article provides insight into the structure of a complicated eclipse bifurcation.

5 Conclusions

A complete analytical solution for the equilibria of 2-DOF twinkling oscillator with a unique bifurcation type has been presented in this paper. The spring mass twinkler consists of nonlinear springs with cubic spring forces, and a quasistatic pull at the end spring. We observed complicated highly degenerate global bifurcations: a local *star* bifurcation (detailed in the previous papers [32, 33]) and global *eclipse* bifurcations. We have shown different symmetry breaking cases for the eclipse bifurcation, which unfolds into saddle-node bifurcations with a general perturbation.

This article gives insight into the dynamics of the 2-DOF twinkling oscillators, hence a building block for further analysis. The unstable branches in the bifurcation plots will not be observable, but understanding them will help in understanding how transient vibrations settle to either of the equilibrium energy levels in symmetry breaking case. Future work will include more detailed study of the existence of chaos through fractal basin boundaries and Lyapunov exponents.

ACKNOWLEDGMENT

This material is based upon work supported by the National Science Foundation under Grant No. CMMI-1030377. Any opinions, findings, and conclusions or recommendations expressed in this material are those of the authors and do not necessarily reflect the views of the National Science Foundation.

REFERENCES

[1] McFarland, D. M., Bergman, L. A., and Vakakis, A. F., 2005. "Experimental study of non-linear energy pumping occurring at a single fast frequency". *International Journal of Non-Linear Mechanics,* ***40***(6), pp. 891–899.

[2] Gourdon, E., Alexander, N. A., Taylor, C. A., Lamarque, C. H., and Pernot, S., 2007. "Nonlinear energy pumping under transient forcing with strongly nonlinear coupling: Theoretical and experimental results". *Journal of Sound and Vibration,* ***300***(3-5), pp. 522–551.

[3] Manevitch, L. I., Musienko, A. I., and Lamarque, C. H.,

2007. "New analytical approach to energy pumping problem in strongly nonhomogeneous 2dof systems". *Meccanica,* ***42***(1), pp. 77–83.

[4] Tsakirtzis, S., Panagopoulos, P. N., Kerschen, G., Gendelman, O., Vakakis, A. F., and Bergman, L. A., 2007. "Complex dynamics and targeted energy transfer in linear oscillators coupled to multi-degree-of-freedom essentially nonlinear attachments". *Nonlinear Dynamics,* ***48***(3), pp. 285–318.

[5] Quinn, D. D., Gendelman, O., Kerschen, G., Sapsis, T. P., Bergman, L. A., and Vakakis, A. F., 2008. "Efficiency of targeted energy transfers in coupled nonlinear oscillators associated with 1:1 resonance captures: Part i". *Journal of Sound and Vibration,* ***311***(3-5), pp. 1228–1248.

[6] Sapsis, T. P., Vakakis, A. F., Gendelman, O. V., Bergman, L. A., Kerschen, G., and Quinn, D. D., 2009. "Efficiency of targeted energy transfers in coupled nonlinear oscillators associated with 1:1 resonance captures: Part ii, analytical study". *Journal of Sound and Vibration,* ***325***(1-2), pp. 297–320.

[7] Vakakis, A., Gendelman, O., Bergman, L., McFarland, D., Kerschen, G., and Lee, Y. S., 2009. *Nonlinear Targeted Energy Transfer in Mechanical and Structural Systems: I and II*. Springer.

[8] Bellet, R., Cochelin, B., Herzog, P., and Mattei, P. O., 2010. "Experimental study of targeted energy transfer from an acoustic system to a nonlinear membrane absorber". *Journal of Sound and Vibration,* ***329***(14), pp. 2768–2791.

[9] Kerschen, G., McFarland, D. M., Kowtko, J. J., Lee, Y. S., Bergman, L. A., and Vakakis, A. F., 2007. "Experimental demonstration of transient resonance capture in a system of two coupled oscillators with essential stiffness nonlinearity". *Journal of Sound and Vibration,* ***299***(4-5), pp. 822–838.

[10] Quinn, D. D., Triplett, A. L., Bergman, L. A., and Vakakis, A. F., 2011. "Comparing linear and essentially nonlinear vibration-based energy harvesting". *Journal of Vibration and Acoustics,* ***133***, p. 011001.

[11] Quinn, D. D., Triplett, A. L., Vakakis, A. F., and Bergman, L. A., 2011. "Energy harvesting from impulsive loads using intentional essential nonlinearities". *Journal of Vibration and Acoustics,* ***133***, p. 011004.

[12] Roundy, S., and Wright, P. K., 2004. "A piezoelectric vibration based generator for wireless electronics". *Smart Materials and Structures,* ***13***, p. 1131.

[13] Sodano, H. A., Inman, D. J., and Park, G., 2005. "Comparison of piezoelectric energy harvesting devices for recharging batteries". *Journal of Intelligent Material Systems and Structures,* ***16***(10), p. 799.

[14] Liao, Y., and Sodano, H. A., 2008. "Model of a single mode energy harvester and properties for optimal power generation". *Smart Materials and Structures,* ***17***, p. 065026.

[15] Renno, J. M., Daqaq, M. F., and Inman, D. J., 2009. "On the optimal energy harvesting from a vibration source". *Journal of Sound and Vibration,* ***320***(1-2), pp. 386–405.

[16] Scruggs, J. T., and Behrens, S., 2011. "Optimal energy harvesting from low-frequency bistate force loadings". *Journal of Vibration and Acoustics,* ***133***, p. 011008.

[17] Anton, S. R., and Sodano, H. A., 2007. "A review of power harvesting using piezoelectric materials (2003–2006)". *Smart Materials and Structures,* ***16***, p. R1.

[18] Stanton, S. C., Erturk, A., Mann, B. P., and Inman, D. J., 2010. "Nonlinear piezoelectricity in electroelastic energy harvesters: Modeling and experimental identification". *Journal of Applied Physics,* ***108***(7), pp. 074903–074903.

[19] Stanton, S. C., McGehee, C. C., and Mann, B. P., 2010. "Nonlinear dynamics for broadband energy harvesting: Investigation of a bistable piezoelectric inertial generator". *Physica D: Nonlinear Phenomena,* ***239***(10), pp. 640–653.

[20] Kim, S., Clark, W. W., and Wang, Q. M., 2005. "Piezoelectric energy harvesting with a clamped circular plate: experimental study". *Journal of Intelligent Material Systems and Structures,* ***16***(10), p. 855.

[21] Mo, C., Radziemski, L. J., and Clark, W. W., 2010. "Experimental validation of energy harvesting performance for pressure-loaded piezoelectric circular diaphragms". *Smart Materials and Structures,* ***19***, p. 075010.

[22] Mann, B. P., and Sims, N. D., 2009. "Energy harvesting from the nonlinear oscillations of magnetic levitation". *Journal of Sound and Vibration,* ***319***(1-2), pp. 515–530.

[23] Priya, S., and Inman, D. J., 2008. *Energy harvesting technologies*. Springer.

[24] Stephen, N. G., 2006. "On energy harvesting from ambient vibration". *Journal of Sound and Vibration,* ***293***(1-2), pp. 409–425.

[25] Feeny, B. F., and Diaz, A. R., 2010. "Twinkling phenomena in snap-through oscillators". *Journal of Vibration and Acoustics,* ***132***, p. 061013.

[26] Wang, Y. C., and Lakes, R. S., 2004. "Extreme stiffness systems due to negative stiffness elements". *American Journal of Physics,* ***72***, p. 40.

[27] Puglisi, G., and Truskinovsky, L., 2000. "Mechanics of a discrete chain with bi-stable elements". *Journal of the Mechanics and Physics of Solids,* ***48***(1), pp. 1–27.

[28] Puglisi, G., and Truskinovsky, L., 2002. "Rate independent hysteresis in a bi-stable chain". *Journal of the Mechanics and Physics of Solids,* ***50***(2), pp. 165–187.

[29] Puglisi, G., 2006. "Hysteresis in multi-stable lattices with non-local interactions". *Journal of the Mechanics and Physics of Solids,* ***54***(10), pp. 2060–2088.

[30] Sarafian, H., 2010. "Static electric-spring and nonlinear oscillations". *Journal of Electromagnetic Analysis & Applications (JEMAA),* ***2***(2), pp. 75–81.

[31] Sarafian, H., 2011. "Nonlinear oscillations of a magneto static spring-mass". *Journal of Electromagnetic Analysis and Applications,* ***3***, pp. 133–139.

[32] Panigrahi, S. R., Feeny, B. F., and Diaz, A. R., 2012. "Bifurcations in twinkling oscillators". *Proceedings of the ASME International Design Engineering Technical Conferences, 24th Conference on Mechanical Vibration and Noise, Chicago, IL, August 12-15, ASME Paper No. DETC2012/VIB-70943*.

[33] Panigrahi, S. R., Feeny, B. F., and Diaz, A. R., 2013. "Degenerate "star" bifurcations in a twinkling oscillator". *Journal of Vibration and Acoustics,* in review.

[34] Nayfeh, A. H., and Balachandran, B., 1995. *Applied nonlinear dynamics: analytical, computational, and experimental methods*. Wiley.

[35] Wiggins, S., 2003. *Introduction to applied nonlinear dynamical systems and chaos*, Vol. 2. Springer.

[36] Yates, R. C., 1947. *"Conics." A Handbook on Curves and Their Properties*. J. W. Edwards, Ann Arbor, MI.

A Appendix

From [36], the conditions for a general quadratic curve

$$av_1^2 + 2bv_1u_2 + cv_2^2 + 2dv_1 + 2fv_2 + g = 0 \tag{18}$$

to be an ellipse are

$$\Delta \neq 0, \quad \mathbf{G} > 0 \quad \text{and} \quad \frac{\Delta}{\mathbf{I}} < 0 \tag{19}$$

where

$$\Delta = \begin{vmatrix} a & b & d \\ b & c & f \\ d & f & g \end{vmatrix}, \quad \mathbf{G} = \begin{vmatrix} a & b \\ b & c \end{vmatrix}, \quad \mathbf{I} = a + c \tag{20}$$

The center (v_1^0, v_2^0) of the ellipse is given by

$$v_1^0 = \frac{ad - bf}{b^2 - ac} \qquad v_2^0 = \frac{af - bd}{b^2 - ac} \tag{21}$$

and the semi axis lengths are

$$\begin{aligned} r_1 &= \sqrt{\frac{2\big(af^2 + cd^2 + gb^2 - 2bdf - acg\big)}{\big(b^2 - ac\big)\Big[\sqrt{(a-c)^2 + 4b^2} - (a+c)\Big]}} \\ r_2 &= \sqrt{\frac{2\big(af^2 + cd^2 + gb^2 - 2bdf - acg\big)}{\big(b^2 - ac\big)\Big[-\sqrt{(a-c)^2 + 4b^2} - (a+c)\Big]}} \end{aligned} \tag{22}$$

In our case $d = f = 0$ results in $\Delta = (ac - b^2)g$, $\mathbf{G} = (ac - b^2)$ and $\mathbf{I} = (a + c)$. We also have $a = c = 1$, $b = -\frac{1}{2}$, and $g = -1$. which gives us $\Delta = -\frac{9}{4} \neq 0$, $\mathbf{G} = \frac{3}{4} > 0$, $\mathbf{I} = 2$, and $\frac{\Delta}{\mathbf{I}} = -\frac{9}{8} < 0$. Hence we have an ellipse with center at $(v_1^0, v_2^0) = (0, 0)$ and semi-axis lengths

$$\begin{aligned} r_1 &= \sqrt{\frac{2g}{\sqrt{(a-c)^2 + 4b^2} - (a+c)}} &&= \sqrt{2} \\ r_2 &= \sqrt{\frac{2g}{-\sqrt{(a-c)^2 + 4b^2} - (a+c)}} &&= \frac{\sqrt{2}}{\sqrt{3}} \end{aligned} \tag{23}$$